DISCRETE TRANSPARENT BOUNDARY CONDITIONS FOR WIDE ANGLE PARABOLIC EQUATIONS IN UNDERWATER ACOUSTICS

ANTON ARNOLD[1,2] AND *MATTHIAS EHRHARDT*[1]

[1]*Fachbereich Mathematik*
TU Berlin, MA 6–2
Straße des 17. Juni 136
D–10623 Berlin, Germany

[2]*Center for Applied Mathematics*
Purdue University
West Lafayette, IN 47907, USA

E–mail: arnold@math.tu-berlin.de, ehrhardt@math.tu-berlin.de

ABSTRACT. This paper is concerned with transparent boundary conditions (TBCs) for wide angle "parabolic" equations (WAPEs) in the application to underwater acoustics (assuming cylindrical symmetry). Existing discretizations of these TBCs introduce slight numerical reflections at this artificial boundary and also render the overall Crank–Nicolson finite difference method only conditionally stable. Here, a novel discrete TBC is derived from the fully discretized whole–space problem that is reflection–free and yields an unconditionally stable scheme. While we shall assume a uniform discretization in range, the interior depth discretization (i.e. in the water column) may be nonuniform, and we shall discuss strategies for the 'best exterior discretization' (i.e. in the sea bottom). The superiority of the new discrete TBC over existing discretizations is illustrated on several benchmark problems.

In the literature different WAPEs (or WAPE and the standard "parabolic" equation) have been coupled in the water and the sea bottom. We analyze under which conditions this yields a hybrid model that is conservative for the acoustic field.

1. Introduction

This paper is concerned with a finite difference discretization of *wide angle "parabolic" equations*. These models appear as one–way approximations to the Helmholtz equation in cylindrical coordinates with azimuthal symmetry. In particular we will discuss the discretization of transparent boundary conditions.

In the past two decades *"parabolic" equation* (PE) models have been widely used for wave propagation problems in various application areas, e.g. seismology [10, 11], optics and plasma physics (cf. the references in [6]). Here we will be mainly interested in their application to underwater acoustics, where PEs have been introduced by Tappert [43]. An account on the vast recent literature is given in the survey article [28].

In oceanography one wants to calculate the underwater acoustic pressure $p(z, r)$ emerging from a time–harmonic point source located in the water at $(z_s, 0)$. Here, $r > 0$ denotes the radial range variable and $0 < z < z_b$ the depth variable. The water surface is at $z = 0$, and the sea bottom at $z = z_b$. In our numerical tests of discrete transparent boundary conditions (in §4) we will only deal with horizontal bottoms. However, irregular bottom surfaces and sub–bottom layers can be included by simply extending the range of z. We denote the local sound speed by $c(z, r)$, the density by $\rho(z, r)$, and the attenuation by $\alpha(z, r) \geq 0$. $n(z, r) = c_0/c(z, r)$ is the refractive index, with a reference sound speed c_0 (usually the smallest sound speed in the model). Then the reference wave number is $k_0 = 2\pi f/c_0$, where f denotes the (usually low) frequency of the emitted sound.

The pressure satisfies the Helmholtz equation

$$\frac{1}{r}\frac{\partial}{\partial r}\left(r\frac{\partial p}{\partial r}\right) + \rho\frac{\partial}{\partial z}\left(\rho^{-1}\frac{\partial p}{\partial z}\right) + k_0^2 N^2 p = 0, \qquad r > 0, \qquad (1.1)$$

with the complex refractive index

$$N(z, r) = n(z, r) + i\alpha(z, r)/k_0. \qquad (1.2)$$

In the far field approximation ($k_0 r \gg 1$) the (complex valued) outgoing acoustic field

$$\psi(z, r) = \sqrt{k_0 r}\, p(z, r)\, e^{-ik_0 r} \qquad (1.3)$$

satisfies the *one–way Helmholtz equation*:

$$\psi_r = ik_0\left(\sqrt{1 - L} - 1\right)\psi, \qquad r > 0. \qquad (1.4)$$

Here, $\sqrt{1 - L}$ is a pseudo–differential operator, and L the Schrödinger operator

$$L = -k_0^{-2}\rho\,\partial_z(\rho^{-1}\partial_z) + V(z, r) \qquad (1.5)$$

with the complex valued "potential" $V(z, r) = 1 - N^2(z, r)$.

The evolution equation (1.4) is much easier to solve numerically than the elliptic Helmholtz equation (1.1). Hence, (1.4) forms the basis for all standard linear models in underwater acoustics (normal mode, ray representation, parabolic equation) [2, 43]. Strictly speaking, (1.4) is only valid for horizontally

stratified oceans, i.e. for range–independent parameters c, ρ, and α. In practice, however, it is still used in situations with weak range dependence, and backscatter is neglected.

"Parabolic" approximations of (1.4) consist in formally approximating the pseudo–differential operator $\sqrt{1-L}$ by rational functions of L, which yields a PDE that is easier to discretize than the pseudo–differential equation (1.4). For a detailed description and motivation of this procedure we refer to [12, 20, 21, 28, 43, 44]. The linear approximation of $\sqrt{1-\lambda}$ by $1-\frac{\lambda}{2}$ gives the narrow angle or *standard "parabolic" equation* (SPE) of Tappert [43]

$$\psi_r = -\frac{ik_0}{2}\, L\psi, \qquad r > 0. \tag{1.6}$$

This Schrödinger equation is a reasonable description of waves with a propagation direction within about 15° of the horizontal. Rational approximations of the form

$$(1-\lambda)^{\frac{1}{2}} \approx f(\lambda) = \frac{p_0 - p_1\lambda}{1 - q_1\lambda} \tag{1.7}$$

with real p_0, p_1, q_1 yield the *wide angle "parabolic" equations* (WAPE)

$$\psi_r = ik_0 \left(\frac{p_0 - p_1 L}{1 - q_1 L} - 1 \right)\psi, \qquad r > 0. \tag{1.8}$$

In the sequel we will repeatedly require the condition

$$f'(0) = p_0 q_1 - p_1 < 0. \tag{1.9}$$

With the choice $p_0 = 1$, $p_1 = \frac{3}{4}$, $q_1 = \frac{1}{4}$ ((1,1)–Padé approximant of $(1-\lambda)^{\frac{1}{2}}$) one obtains the WAPE of Claerbout [10]. In [21] Greene determines these coefficients by minimizing the approximation error of $(1-\lambda)^{\frac{1}{2}}$ over suitable λ–intervals. These WAPE models furnish a much better description of the wave propagation up to angles of about 40°. Also, higher order analogues of (1.7), (1.8) [14, 23] and split–step Padé algorithms [15] have been successfully used for acoustic problems. While we will restrict ourselves here to the WAPE (1.8), we remark that the construction of discrete transparent boundary conditions (see §3) could be generalized to higher order PEs and even 3D–problems.

In this article we shall focus on boundary conditions (BC) for the WAPE (1.8). At the water surface one usually employs a Dirichlet ("pressure release") BC: $\psi(z = 0, r) = 0$. At the sea bottom the wave propagation in water has to be coupled to the wave propagation in the sediments of the bottom. The bottom will be modeled as the homogeneous half–space region $z > z_b$ with constant parameters c_b, ρ_b, and α_b. Throughout most of this paper we will use a fluid model for the bottom by assuming that (1.8) also holds for $z > z_b$, possibly with a different rational approximation (1.7) (subject to the *coupling condition* (2.23)). Only at the end of §2 we will comment on the coupling of scalar and elastic "parabolic" models.

In practical simulations one is only interested in the acoustic field $\psi(z, r)$ in the water, i.e. for $0 < z < z_b$. While the physical problem is posed on the unbounded z–interval $(0, \infty)$, one wishes to restrict the computational domain in

the z–direction by introducing an artificial boundary at or below the sea bottom. This artificial BC should of course change the model as little as possible. Until recently, the standard strategy was to introduce rather thick absorbing layers below the sea bottom and then to limit the z–range by again imposing a Dirichlet BC [12, 14, 29, 34, 44]. With a carefully designed absorption profile and layer thickness this strategy has been very successful. But without a comparison to the exact half-space solution it is hard to estimate how much an absorbing layer modifies the original problem. Also, absorbing layers increase the computational costs, for SPE– or WAPE–simulations typically by a factor around 2 [28, 45]. However, in simulations without attenuation ("false absorbing layer method" [28, 45]) or over an elastic sea bottom [14], much thicker absorbing layers have been used to ensure accuracy and, respectively, numerical stability.

In [35] and [37] Papadakis derived *impedance BCs* or *transparent boundary conditions* (TBC) for the SPE and the WAPE, which completely solves the problem of restricting the z–domain without changing the physical model: complementing the WAPE (1.8) with a TBC at z_b allows to recover — on the finite computational domain $(0, z_b)$ — the exact half–space solution on $0 < z < \infty$. As the SPE is a Schrödinger equation, similar strategies have been developed independently for quantum mechanical applications [5, 7, 24].

Towards the end of this introduction we shall now turn to the main motivation of this paper. While TBCs fully solve the problem of cutting off the z–domain for the analytical equation, their numerical discretization is far from trivial. Indeed, all available discretizations are less accurate than the discretized half–space problem and they render the overall numerical scheme only conditionally stable [7, 33, 36, 45]. The object of this paper is to construct *discrete transparent boundary conditions* (DTBC) for a Crank–Nicolson finite difference discretization of the WAPE such that the overall scheme is unconditionally stable and as accurate as the discretized half–space problem.

The paper is organized as follows: In §2 we review the TBCs for the WAPE and discuss the coupling of the WAPE to the SPE and the elastic PE. In §3 discrete TBCs are derived and analyzed; their superiority over existing discretizations is illustrated in the numerical tests of §4.

2. Transparent Boundary Conditions and Model Coupling

In this Section we shall first discuss the well–posedness of the evolution problem for the WAPE in the critical non–dissipative case, i.e. for $\alpha = 0$:

$$\psi_r = ik_0\big[f(L) - 1\big]\psi, \qquad z > 0, \quad r > 0, \tag{2.1}$$

subject to the BC $\psi(0, r) = 0$, and with the rational function f given in (1.7). For simplicity of the analysis we only consider the range–independent situation; the functional analytic proof of this theorem is deferred to the Appendix.

Theorem 1. *Assume that the refractive index $n(z)$, the density $\rho(z) > 0$, and $\rho^{-1}(z)$ are bounded for $z > 0$. Then, the WAPE has a unique solution for all initial data in the weighted L^2–space $L^2(\mathbb{R}^+; \rho^{-1}dz)$ if and only if the pole of*

$f(\lambda)$ at $\tilde{\lambda} = q_1^{-1}$ *is not an eigenvalue of the operator L with Dirichlet BCs at* $z = 0$.

In applications of underwater acoustics the sound speed $c(z)$ is typically larger in the sea bottom than in the water. Therefore $V(z)$ forms a "potential well" in the water region $0 < z < z_b$, which typically gives rise to bound states of L that represent the propagating modes of (1.4) and (1.8). All of the corresponding eigenvalues satisfy $0 < \lambda_j < V_b = 1 - c_0^2/c_b^2 < 1$, if $c_0 = \min_{z>0} c(z)$. As q_1 is much smaller than 1 in all practical simulations ($\frac{1}{4}$ in the WAPE of Claerbout; also cf. [21]), $\tilde{\lambda}$ usually lies in $[V_b, \infty)$, the continuous spectrum of L. Theorem 1 then guarantees the unique solvability of the evolution equation (2.1) for any initial data. Let us compare the situation at hand (i.e. the WAPE on the original unbounded interval — and later also the WAPE with a TBC) to the WAPE restricted to the z–interval $[0, z_{max}]$ with a homogeneous Robin BC at z_{max} as a simple model for an absorbing layer: there, L has a pure eigenvalue spectrum which inhibits the solvability of (2.1) in several cases of practical relevance [3].

Now we turn to the matching conditions and later the TBCs at the water–bottom interface ($z = z_b$). As the density is typically discontinuous there, one requires continuity of the pressure and the normal particle velocity:

$$\psi(z_{b-}, r) = \psi(z_{b+}, r), \tag{2.2a}$$

$$\frac{\psi_z(z_{b-}, r)}{\rho_w} = \frac{\psi_z(z_{b+}, r)}{\rho_b}, \tag{2.2b}$$

where $\rho_w = \rho(z_{b-}, r)$ is the water density just above the bottom and ρ_b denotes the constant density of the bottom.

With these matching conditions we shall now derive an estimate for the L^2–decay of solutions to the WAPE (1.8), $z > 0$. We assume $\rho = \rho(z)$ and apply the operator $1 - q_1 L$ to (1.8):

$$\left[1 - q_1 V + q_1 k_0^{-2} \rho \, \partial_z (\rho^{-1} \partial_z) \right] \psi_r$$
$$= i k_0 \left[p_0 - 1 - (p_1 - q_1) V + (p_1 - q_1) k_0^{-2} \rho \, \partial_z (\rho^{-1} \partial_z) \right] \psi. \tag{2.3}$$

Multiplying (2.3) by $\bar{\psi} \rho^{-1}$, integrating by parts on $0 < z < z_b$, and taking the real part gives

$$\partial_r \int_0^{z_b} |\psi|^2 \, \rho^{-1} dz$$
$$= 2(p_1 - q_1) k_0 \left\{ \int_0^{z_b} \mathrm{Im}\,[V] \, |\psi|^2 \, \rho^{-1} dz - k_0^{-2} \rho_w^{-1} \, \mathrm{Im}\, \left[\psi_z \bar{\psi} \right] \big|_{z=z_b-} \right\}$$
$$+ q_1 \left\{ \int_0^{z_b} \left(\mathrm{Re}\,[V] \partial_r \, |\psi|^2 - 2\,\mathrm{Im}\,[V]\,\mathrm{Im}\,[\psi_r \bar{\psi}] \right) \rho^{-1} dz \right.$$
$$\left. + k_0^{-2} \partial_r \int_0^{z_b} |\psi_z|^2 \, \rho^{-1} dz - 2 k_0^{-2} \rho_w^{-1} \, \mathrm{Re}\, \left[\psi_{zr} \bar{\psi} \right] \big|_{z=z_b-} \right\}. \tag{2.4}$$

5

Analogously, multiplying (2.3) by $\bar{\psi}_r \rho^{-1}$, and taking the imaginary part we get

$$(p_0 - 1)\partial_r \int_0^{z_b} |\psi|^2 \rho^{-1} dz$$

$$= -2q_1 k_0^{-1} \int_0^{z_b} \text{Im}\,[V]\,|\psi_r|^2\,\rho^{-1} dz + 2q_1 k_0^{-3} \rho_w^{-1}\,\text{Im}\,\left[\psi_{zr}\bar{\psi}_r\right]\Big|_{z=z_b-}$$

$$+ (p_1 - q_1)\left\{\int_0^{z_b} \left(\text{Re}\,[V]\partial_r\,|\psi|^2 + 2\,\text{Im}\,[V]\,\text{Im}\,[\psi_r\bar{\psi}]\right)\rho^{-1} dz\right.$$

$$\left. + k_0^{-2}\partial_r \int_0^{z_b} |\psi_z|^2\,\rho^{-1} dz - 2k_0^{-2}\rho_w^{-1}\,\text{Im}\,\left[\psi_z\bar{\psi}_r\right]\Big|_{z=z_b-}\right\}. \tag{2.5}$$

After an easy algebraic manipulation we obtain from (2.4), (2.5)

$$\partial_r \int_0^{z_b} |\psi|^2\,\rho^{-1}\,dz$$

$$= -2C_1 \int_0^{z_b} \alpha\,\frac{c_0}{c}\,\left|\tilde{\partial}_r\psi\right|^2\,\rho^{-1}\,dz - C_1 k_0^{-1}\rho_w^{-1}\,\text{Im}\,\left[\tilde{\partial}_r\psi_z\overline{\tilde{\partial}_r\psi}\right]\Big|_{z=z_b-}, \tag{2.6}$$

with

$$C_1 = \frac{2(p_1 - q_1)^2}{p_1 - p_0 q_1}, \qquad \tilde{\partial}_r = I + \frac{iq_1}{p_1 - q_1}k_0^{-1}\partial_r.$$

In the same way a similar equation can be derived for the bottom region $z > z_b$:

$$\partial_r \int_{z_b}^{\infty} |\psi|^2\,\rho^{-1}\,dz$$

$$= -2C_1\alpha_b\,\frac{c_0}{c_b}\int_{z_b}^{\infty}\left|\tilde{\partial}_r\psi\right|^2\,\rho^{-1}\,dz + C_1 k_0^{-1}\rho_b^{-1}\,\text{Im}\,\left[\tilde{\partial}_r\psi_z\overline{\tilde{\partial}_r\psi}\right]\Big|_{z=z_b+}. \tag{2.7}$$

Adding the two above equations with (2.2) gives

$$\partial_r \|\psi(.,r)\|^2 = -2C_1 \int_0^{\infty} \alpha\,\frac{c_0}{c}\,\left|\tilde{\partial}_r\psi\right|^2\,\rho^{-1}\,dz \tag{2.8}$$

for the weighted L^2–norm

$$\|\psi(.,r)\|^2 = \int_0^{\infty} |\psi(z,r)|^2\,\rho^{-1}(z)\,dz. \tag{2.9}$$

In the dissipation–free case ($\alpha \equiv 0$) $\|\psi(.,r)\|$ is conserved and for $\alpha > 0$ and $p_0 q_1 - p_1 < 0$ it decays. The discrete analogue of this "energy"–conservation (or –decay for $\alpha > 0$) will be the main ingredient for showing unconditional stability of the finite difference scheme in §3.

Now we shall review the transparent bottom boundary condition for the SPE and sketch the derivation of the TBC for the WAPE. We assume that the initial data $\psi^I = \psi(z,0)$, which models a point source located at $(z_s, 0)$, is supported in the *interior domain* $0 < z < z_b$. Also, let the bottom region be homogenous, let i.e. all physical parameters be constant for $z > z_b$. The basic idea of the derivation is to explicitly solve the equation in the bottom region, which is the exterior of the computational domain $(0, z_b)$. The TBC for the

SPE (or Schrödinger equation) was derived in [5, 7, 24, 33, 35, 37] for various application fields:

$$\psi(z_b, r) = -(2\pi k_0)^{-\frac{1}{2}} e^{\frac{\pi}{4}i} \frac{\rho_b}{\rho_w} \int_0^r \psi_z(z_b, r - \tau) e^{ib\tau} \tau^{-\frac{1}{2}} d\tau, \qquad (2.10)$$

with $b = k_0(N_b^2 - 1)/2$. This BC is nonlocal in the range variable r and involves a mildly singular convolution kernel. Equivalently, it can be written as

$$\psi_z(z_b, r) = -\left(\frac{2k_0}{\pi}\right)^{\frac{1}{2}} e^{-\frac{\pi}{4}i} e^{ibr} \frac{\rho_w}{\rho_b} \frac{d}{dr} \int_0^r \psi(z_b, \tau) e^{-ib\tau} (r - \tau)^{-\frac{1}{2}} d\tau, \quad (2.11)$$

and the r.h.s. can be expressed formally as a fractional $(\frac{1}{2})$ derivative [5, 7, 9]:

$$\psi_z(z_b, r) = -\sqrt{2k_0} e^{-\frac{\pi}{4}i} e^{ibr} \frac{\rho_w}{\rho_b} \partial_r^{1/2} \left[\psi(z_b, r) e^{-ibr}\right]. \qquad (2.12)$$

In [9] this square root operator is approximated by rational functions which leads to a hierarchy of *highly absorbing* (but not any more perfectly transparent) *BCs* for the SPE. By introducing auxiliary boundary variables these BCs can be expressed through local–in–r operators. Hence, this allows for a "local" (2–level in r) discretization scheme [16]. This scheme, however, introduces numerical reflections at the artificial boundary, whose amplitude depends on the chosen approximation order of the above square root operator.

In order to derive the TBC for the WAPE we consider (2.3) in the bottom region:

$$(\delta_b + q_1 k_0^{-2} \partial_z^2)\psi_r = i\left[v_b + (p_1 - q_1)k_0^{-1}\partial_z^2\right]\psi, \qquad z > z_b, \qquad (2.13)$$

with

$$\delta_b = 1 - q_1(1 - N_b^2), \quad v_b = k_0\left[p_0 - 1 - (p_1 - q_1)(1 - N_b^2)\right].$$

After a Laplace transformation of (2.13) in r we get

$$\left[q_1 s - i(p_1 - q_1)k_0\right]\hat{\psi}_{zz}(z, s) = k_0^2(iv_b - \delta_b s)\hat{\psi}(z, s). \qquad (2.14)$$

Since its solution has to decay as $z \to \infty$ we obtain

$$\hat{\psi}(z, s) = \hat{\psi}(z_{b+}, s) \exp\left\{-k_0 \sqrt[+]{\frac{iv_b - \delta_b s}{q_1 s - i(p_1 - q_1)k_0}} (z - z_b)\right\}, \quad z > z_b, \quad (2.15)$$

and with the matching conditions (2.2) this gives

$$\hat{\psi}_z(z_{b-}, s) = -k_0 \frac{\rho_w}{\rho_b} \sqrt[+]{\frac{iv_b - \delta_b s}{q_1 s - i(p_1 - q_1)k_0}} \hat{\psi}(z_{b-}, s). \qquad (2.16)$$

Here, $\sqrt[+]{}$ denotes the branch of the square root with a nonnegative real part. An inverse Laplace transformation [8] yields the TBC at the bottom for the WAPE:

$$\psi(z_b, r) = -i\eta \frac{\rho_b}{\rho_w} \psi_z(z_b, r)$$
$$+ \beta \eta \frac{\rho_b}{\rho_w} \int_0^r \psi_z(z_b, r - \tau) e^{i\theta\tau} e^{i\beta\tau} \left[J_0(\beta\tau) + iJ_1(\beta\tau)\right] d\tau, \quad (2.17)$$

$$\eta = \frac{1}{k_0} \sqrt[+]{\frac{q_1}{\delta_b}}, \quad \beta = -\frac{p_1 - p_0 q_1}{2 q_1} \frac{k_0}{\delta_b}, \quad \theta = \frac{p_1 - q_1}{q_1} k_0,$$

where J_0, J_1 denote the Bessel functions of order 0 and 1, respectively. This is a slight generalization of the TBC derived in [37] where p_0 was equal to 1. Equivalently, (2.17) can be written as

$$\psi_z(z_b, r) = i\eta^{-1} \frac{\rho_w}{\rho_b} \psi(z_b, r)$$

$$+ \beta \eta^{-1} \frac{\rho_w}{\rho_b} \int_0^r \psi(z_b, r - \tau) e^{i\theta\tau} e^{i\beta\tau} \left[J_0(\beta\tau) - iJ_1(\beta\tau) \right] d\tau. \quad (2.18)$$

Both TBCs are non–local in r; in range marching algorithms they thus require storing the bottom boundary data of all previous range levels.

We remark that the asymptotic behaviour (for $r \to \infty$) of the convolution kernel in the TBC (2.11) is $O\left(r^{-3/2}\right)$, which can be seen after an integration by parts. Using the asymptotic behaviour of the Bessel functions (see (3.5)) one finds that the convolution kernel of (2.18) also decays like $O\left(r^{-3/2}\right)$.

At the end of this Section we shall now briefly comment on coupled models for underwater acoustics, as proposed in [36, 37]. In [37] the WAPE for the ocean $(0 < z < z_b)$ is coupled to the SPE for the sea bottom $(z > z_b)$. In fact, these models are coupled via a TBC corresponding to the SPE, but this is equivalent to the half–space problem. Here we want to point out a mathematical ambiguity of this coupling that may strongly influence the numerical stability of the discretization scheme. To this end we consider this model coupling in the case of constant sound speed and density, which is rather unrealistic, but it illustrates the situation.

Let us first review the WAPE (2.1) with the Schrödinger operator $L = -k_0^{-2}\partial_z^2$. When discretizing (2.1) one usually applies the operator $1 - q_1 L$ to (2.1) which gives the following PDE of "Sobolev type" [27]

$$\left[(1 - q_1 L)\psi_r = ik_0 \left[p_0 - 1 - (p_1 - q_1)L\right]\psi. \quad (2.19)$$

Since the operators in the numerator and denominator of (1.8) commute (even for non–constant c and ρ) this step is mathematically rigorous, and (2.19) is easy to discretize (see §3).

Disregarding for the moment the nonlocality of the involved pseudo–differential operator, one would formally want to write the evolution equation for the coupled model (WAPE and SPE) as

$$\psi_r = ik_0 A\psi \quad (2.20)$$

with

$$A\psi = \begin{cases} \left(\dfrac{p_0 + p_1 k_0^{-2}\partial_z^2}{1 + q_1 k_0^{-2}\partial_z^2} - 1\right)\psi, & 0 < z < z_b, \quad (2.21a) \\[3mm] \dfrac{k_0^{-2}}{2}\partial_z^2 \psi, & z > z_b. \quad (2.21b) \end{cases}$$

However, the right hand side of (2.20) is not well–defined, due to the non–locality of the pseudo–differential operator in (2.21a). Also, its reformulation as in (2.19) is not any longer justified in the coupled case. Even in the

dissipation–free case it would result in a non–conservative evolution equation and hence in a non–conservative numerical scheme (nevertheless this strategy is used in [37]). This is illustrated in Example 3 of §4. Using more involved pseudo–differential operators it is possible to find a correct and conservative interpretation of (2.20), (2.21) (for mathematical details see Appendix B). However, its discretization would be very difficult.

From the above we conclude that it is not advisable to couple the WAPE and the SPE numerically. As an alternative we shall now analyze couplings of WAPEs with different parameters p_0, p_1, q_1 that can be reformulated as a PDE, like in (2.19). The coupled model

$$\psi_r = ik_0 \left(\frac{p_0(z) - p_1(z)L}{1 - q_1(z)L} - 1 \right) \psi \tag{2.22}$$

is well–defined and can be transformed to (2.19) if the numerator and denominator in (2.22) commute. Under the condition

$$p_1(z)/q_1(z) =: \mu = \mathrm{const} \tag{2.23}$$

we can rewrite the pseudo–differential operator in (2.22) as

$$\frac{p_0(z) - p_1(z)L}{1 - q_1(z)L} = \frac{\mu \big[\tau(z) - \mu^{-2}\sigma(z)L \big] - 1}{\tau(z) - \mu^{-2}\sigma(z)L}, \tag{2.24}$$

with

$$\tau(z) = \big[\mu - p_0(z) \big]^{-1}, \quad \sigma(z) = p_1^2(z)\big[p_1(z) - p_0(z)q_1(z) \big]^{-1}. \tag{2.25}$$

Here the numerator and denominator commute, and hence (2.22) can be written in the form of (2.19). The resulting evolution equation is conservative in $L^2(\mathbb{R}^+; (\sigma\rho)^{-1}dz)$ and it allows for a conservative and unconditionally stable discretization (see §3 and Example 3 in §4).

If the parameters p_0, p_1, q_1 are fixed in one medium, condition (2.23) still leaves two free parameters to choose a different rational approximation model of $(1 - \lambda)^{\frac{1}{2}}$ for the second medium (cp. [21]). Hence, one can in fact obtain a better approximation in the second medium than with the originally intended "parabolic approximation".

Finally we add a small remark on the coupling of the SPE with an *elastic parabolic equation* (EPE) for the sea bottom [13, 22, 47]. In [36, 37] a TBC for this coupling was derived. It reads for the Laplace transformed wave field:

$$\hat{\psi}(z_b, s) = -\frac{\rho_b}{\rho_w} \frac{1}{k_0 N_s^4} \frac{1}{\sqrt[+]{M_p(s)}} \times$$

$$\times \left[\big(2M_s(s) + N_s^2 \big)^2 - 4 \sqrt[+]{M_p(s)} \sqrt[+]{M_s(s)} \big(M_s(s) + N_s^2 \big) \right] \hat{\psi}_z(z_b, s), \quad (2.26)$$

with the notation

$$M_p(s) = 1 - N_p^2 - \frac{2i}{k_0}s, \quad M_s(s) = 1 - N_s^2 - \frac{2i}{k_0}s. \tag{2.27}$$

Here, $N_p = n_p + i\alpha_p/k_0$ and $N_s = n_s + i\alpha_s/k_0$ denote the complex refractive indices for the compressional and shear waves in the bottom (cp. (1.2)). In a

9

tedious calculation this BC can indeed be inverse Laplace transformed (using [8]) and it reads:

$$\psi(z_b, r) =$$
$$C\left[\int_0^r \psi_z(z_b, r - \tau)\, e^{i\omega\tau} g(\tau)\, d\tau - 2i\varphi \int_0^r \psi_{zr}(z_b, r - \tau)\, e^{i\omega\tau} \tau^{-\frac{1}{2}}\, d\tau\right], \quad (2.28)$$

with

$$C = -\frac{\rho_b}{\rho_w}\frac{2}{k_0^{5/2} N_s^4}\sqrt{\frac{2}{\pi}}\, e^{\frac{\pi}{4}i}, \quad \omega = \frac{k_0}{2}\big(N_p^2 - 1\big), \quad \varphi = -\frac{k_0}{2}\big(N_p^2 - N_s^2\big),$$

$$g(\tau) = -3\big(1 - e^{i\varphi\tau}\big)\tau^{-\frac{5}{2}} + i\frac{k_0}{2}\big(3N_p^2 - N_s^2 - 2N_s^2 e^{i\varphi\tau}\big)\tau^{-\frac{3}{2}} +$$
$$\frac{k_0^2}{2}\big(N_p^4 - N_p^2 N_s^2 + \tfrac{1}{2}N_s^4 + N_p^2 - N_s^2\big)\tau^{-\frac{1}{2}} = O\big(\tau^{-\frac{1}{2}}\big).$$

While this inverse transformation was carried out numerically in [36, 37], our analytical TBC may simplify the discretization of this coupled model. DTBCs for the SPE–EPE coupling (in the spirit of §3) will be the topic of a subsequent paper.

3. Discrete Transparent Boundary Conditions

In this Section we shall discuss how to discretize the TBCs (2.10), (2.17) in conjunction with a Crank–Nicolson finite difference scheme for the SPE and the WAPE. Most of the time we shall only consider uniform grids in z and r. While a uniform range discretization is crucial for our construction of discrete TBCs, this construction is independent of the (possibly nonuniform) z–discretization on the interior domain.

For simplicity we first consider the uniform grid $z_j = jh$, $r_n = nk$ ($h = \Delta z$, $k = \Delta r$) and the approximation $\psi_j^n \sim \psi(z_j, r_n)$. The discretized WAPE (2.3) then reads:

$$\left[1 - q_1 V_j^{n+\frac{1}{2}} + q_1 k_0^{-2}\rho_j D_{\frac{h}{2}}^0\big(\rho_j^{-1} D_{\frac{h}{2}}^0\big)\right] D_k^+ \psi_j^n$$
$$= ik_0\left[p_0 - 1 - (p_1 - q_1)V_j^{n+\frac{1}{2}} + (p_1 - q_1)k_0^{-2}\rho_j D_{\frac{h}{2}}^0\big(\rho_j^{-1} D_{\frac{h}{2}}^0\big)\right]\frac{\psi_j^n + \psi_j^{n+1}}{2},$$
$$(3.1)$$

with $V_j^{n+\frac{1}{2}} := V(z_j, r_{n+\frac{1}{2}})$ and the usual difference operators

$$D_k^+ \psi_j^n = \frac{\psi_j^{n+1} - \psi_j^n}{k}, \qquad D_{\frac{h}{2}}^0 \psi_j^n = \frac{\psi_{j+\frac{1}{2}}^n - \psi_{j-\frac{1}{2}}^n}{h}.$$

It is well known that this scheme is second order in h and k and unconditionally stable [3]. Proceeding similarly to the derivation of (2.8) one can

show

$$D_k^+ \sum_{j \in \mathbb{Z}} \frac{\left|\psi_j^n\right|^2}{\rho_j} = -C_1 k_0^{-1} \sum_{j \in \mathbb{Z}} \operatorname{Im} \left\{ V_j^{n+\frac{1}{2}} \right\} \left| \psi_j^{n+\frac{1}{2}} + \frac{iq_1}{p_1 - q_1} k_0^{-1} D_k^+ \psi_j^n \right|^2 \frac{1}{\rho_j},$$

(3.2)

with $C_1 = 2(p_1 - q_1)^2/(p_1 - p_0 q_1)$. Hence, the scheme (3.1) preserves the discrete weighted L^2–norm in the dissipation–free case (V real). This also holds when using a homogeneous Dirichlet BC at $j = 0$.

In the literature three different strategies have been proposed to discretize TBCs, mostly, however, just for the Schrödinger equation: In [45] Thomson and Mayfield used the following *discretized TBC* for the SPE:

$$\psi_J^n - \psi_{J-1}^n = \frac{h}{2Bk^{\frac{1}{2}}} \psi_J^n - B' \sum_{m=1}^{n-1} \left(\psi_J^{n-m} - \psi_{J-1}^{n-m} \right) \hat{\ell}_m,$$

(3.3)

with

$$B = -(2\pi k_0)^{-\frac{1}{2}} e^{\frac{\pi}{4} i} \frac{\rho_b}{\rho_w}, \quad B' = e^{\frac{i}{2} bk} \frac{\sin\left(\frac{1}{2} bk\right)}{\frac{1}{2} bk}, \quad \hat{\ell}_m = \frac{e^{ibmk}}{2\sqrt{m + \frac{1}{2}}}.$$

On the fully discrete level this BC is not perfectly transparent any more and it may also yield an unstable numerical scheme. In analogy to the analytic TBC (2.10) it requires the boundary data from the whole "past range" $[0, r_{n-1}]$.

In the *semi–discrete approach* of Schmidt and Deuflhard [39] a TBC is derived for the semi–discretized (in r) SPE, which also applies for nonuniform r–discretizations and range–dependent coefficients in the exterior domain. This TBC yields an unconditionally stable method (in conjunction with an interior finite element scheme) [40]. In [40] this approach is also applied to uniform exterior z–discretizations, and one then recovers — through a different derivation — the discrete TBC from [5]. While the semi–discrete approach still exhibits small residual reflections at the artificial boundary, the discrete TBC is reflection–free [40] (at the end of this Section we shall return to this comparison when discussing the 'best exterior discretization'). In the recent article [41] the methods of [40] are extended to nonuniform r–discretizations and range–dependent potentials.

In [5] we constructed a *discrete TBC* for the fully discretized Schrödinger equation and the resulting scheme elliminates any numerical reflections. The same strategy was used in [19] for advection diffusion equations and in [17] for the wave equation in frequency domain.

Here we shall generalize the latter approach (i.e. fully DTBC) to the WAPE and compare it numerically to the discretized TBC. To this end we use a

discretization of the TBC (2.17) for the WAPE that is analogous to (3.3):

$$\int_0^r \psi_z(z_b, r_n - \tau) \, e^{i\theta\tau} e^{i\beta\tau} \left[J_0(\beta\tau) + i J_1(\beta\tau) \right] d\tau$$

$$= \sum_{m=0}^{n-1} \int_{r_m}^{r_{m+1}} \psi_z(z_b, r_n - \tau) \, e^{i\theta\tau} \left[\widetilde{J}_0(\beta\tau) + i\widetilde{J}_1(\beta\tau) \right] d\tau$$

$$\approx \sum_{m=0}^{n-1} \frac{\psi_J^{n-m} - \psi_{J-1}^{n-m}}{h} \left[\widetilde{J}_0(\beta r_{m+\frac{1}{2}}) + i\widetilde{J}_1(\beta r_{m+\frac{1}{2}}) \right] \int_{r_m}^{r_{m+1}} e^{i\theta\tau} \, d\tau,$$

with the *damped Bessel functions* $\widetilde{J}_\nu(z) := e^{iz} J_\nu(z)$, $z \in \mathbb{C}$. This yields the following discretized TBC:

$$\psi_J^n - \psi_{J-1}^n = \frac{ih}{\eta} \frac{\rho_w}{\rho_b} \psi_J^n - B' \sum_{m=0}^{n-1} \left(\psi_J^{n-m} - \psi_{J-1}^{n-m} \right) \tilde{\ell}_m, \tag{3.4}$$

with

$$B' = i\beta \, e^{\frac{i}{2}\theta k} \frac{\sin(\frac{1}{2}\theta k)}{\frac{1}{2}\theta}, \quad \tilde{\ell}_m = e^{i\theta mk} \left[\widetilde{J}_0(\beta r_{m+\frac{1}{2}}) + i\widetilde{J}_1(\beta r_{m+\frac{1}{2}}) \right].$$

In far field simulations one has to evaluate $J_\nu(z)$ for large complex z, when numerically calculating these convolution coefficients $\tilde{\ell}_n$. This, however, is a rather delicate problem, and many standard software routines are not able to evaluate $J_\nu(z)$ for large complex z. This is due to the exponential growth of the Bessel functions for fixed ν and $|z| \to \infty$ (see [1]):

$$J_\nu(z) = \left(\frac{2}{\pi z} \right)^{\frac{1}{2}} \left\{ \cos\left(z - \nu\frac{\pi}{2} - \frac{\pi}{4} \right) + e^{|\text{Im } z|} \, \text{O}\big(|z|^{-1}\big) \right\}, \quad -\pi < \arg z < \pi. \tag{3.5}$$

For this reason we used a subroutine of Amos [4] to evaluate the damped Bessel functions $\widetilde{J}_\nu(z)$, $\text{Im } z \geq 0$ (note that $\text{Im } \beta \geq 0$ for the standard parameter choices in (1.7): $p_1 - p_0 q_1 > 0$ and $q_1 > 0$).

In [33] Mayfield showed for the attenuation–free case that the *discretized TBC* for the SPE (3.3) destroys the unconditional stability of the underlying Crank–Nicolson scheme and one can expect a similar behaviour for the WAPE. These existing discretizations also induce numerical reflections at the boundary, particularly when using coarse grids. Hence, the existing *discretized TBC* [33, 45] exhibits both stability problems and reduced accuracy, which may require the usage of unnecessarily fine grids.

Instead of using an ad–hoc discretization of the analytic TBCs like (3.3) or (3.4) we will construct *discrete TBCs* for the fully discretized half–space problem, as done in [5]. Our new strategy solves both problems of the *discretized TBC* at no additional computational costs. With our DTBC the numerical solution on the computational domain $0 \leq j \leq J$ exactly equals the discrete half–space solution (on $j \in \mathbb{N}_0$) restricted to the computational domain $0 \leq j \leq J$. Therefore, our overall scheme inherits the unconditional stability of the half–space solution that is implied by the discrete L^2–estimate (3.2).

12

To derive the DTBC we will now mimic the derivation of the analytic TBCs from §2 on a discrete level. For the initial data we assume $\psi_j^0 = 0$, $j \geq J - 1$ and solve the discrete exterior problem in the bottom region, i.e. the Crank–Nicolson finite difference scheme (3.1) for $j \geq J$:

$$\left[R\delta_b + q\Delta_h^2\right](\psi_j^{n+1} - \psi_j^n) = i\left[R\kappa_b + \Delta_h^2\right](\psi_j^{n+1} + \psi_j^n), \qquad (3.6)$$

with

$$\delta_b = 1 - q_1(1 - N_b^2), \quad R = \frac{2k_0}{p_1 - q_1}\frac{h^2}{k}, \quad q = \frac{k}{2}\frac{q_1}{p_1 - q_1}k_0^{-1},$$

$$\kappa_b = \frac{k}{2}k_0\left[p_0 - 1 - (p_1 - q_1)(1 - N_b^2)\right],$$

where $\Delta_h^2\psi_j^n = \psi_{j+1}^n - 2\psi_j^n + \psi_{j-1}^n$, and R is proportional to the parabolic mesh ratio. By using the Z–transform:

$$\mathcal{Z}\{\psi_j^n\} = \hat{\psi}_j(z) := \sum_{n=0}^{\infty}\psi_j^n z^{-n}, \quad z \in \mathbb{C}, \quad |z| > 1, \qquad (3.7)$$

(3.6) is transformed to

$$\left[z + 1 + iq(z - 1)\right]\Delta_h^2\hat{\psi}_j(z) = -iR\left[\delta_b(z - 1) - i\kappa_b(z + 1)\right]\hat{\psi}_j(z). \qquad (3.8)$$

The solution of the resulting second order difference equation takes the form $\hat{\psi}_j(z) = \nu_1^j(z)$, $j \geq J$, where $\nu_1(z)$ solves

$$\nu^2 - 2\left[1 - \frac{iR}{2}\frac{\delta_b(z - 1) - i\kappa_b(z + 1)}{z + 1 + iq(z - 1)}\right]\nu + 1 = 0. \qquad (3.9)$$

For the decreasing mode (as $j \to \infty$) we require $|\nu_1(z)| < 1$. We obtain the Z–transformed DTBC as

$$\hat{\psi}_{J-1}(z) = \nu_1^{-1}(z)\hat{\psi}_J(z), \qquad (3.10)$$

and in a tedious calculation this can be inverse transformed explicitly. The DTBC for the SPE and the WAPE then reads:

$$(1 + iq)\psi_{J-1}^n = \psi_J^n * \ell_n = \sum_{m=1}^{n}\psi_J^m\ell_{n-m}, \quad n \geq 1, \qquad (3.11)$$

with the convolution coefficients $\ell_n := (1 + iq)\mathcal{Z}^{-1}\{\nu_1^{-1}(z)\}$ given by

$$\ell_n = \left[1 + iq + \frac{i}{2}(\gamma - i\sigma)e^{-i\xi}\right]\delta_n^0 - \frac{i}{2}H(-1)^n e^{in\xi}$$

$$- \zeta\left\{Q_n(\mu) + e^{-i\xi}\lambda^{-2}Q_{n-1}(\mu) + \omega e^{-i\varphi}\sum_{m=0}^{n-1}(-e^{i\xi})^{n-m}Q_m(\mu)\right\}, \qquad (3.12)$$

$$\gamma = R\,\delta_b, \quad \sigma = -R\,\kappa_b, \quad \lambda = \sqrt[+]{\frac{E}{G}}, \quad \mu = \frac{F}{\sqrt[+]{EG}}, \quad \omega = \frac{H^2}{|E|},$$

$$\xi = \arg\frac{1 - iq}{1 + iq}, \quad \varphi = \arg E, \quad \zeta = \frac{i}{2}|E|^{\frac{1}{2}}e^{i\frac{\varphi}{2}},$$

$$E = (\gamma + i\sigma)\left[\gamma - 4q + i(\sigma + 4)\right], \quad F = \gamma(\gamma - 4q) + \sigma(\sigma + 4),$$

$$G = (\gamma - i\sigma)\big[\gamma - 4q - i(\sigma + 4)\big], \quad H = \gamma + i\sigma + (\gamma - i\sigma)e^{-i\xi}.$$

In (3.12) δ_n^0 denotes the Kronecker symbol and $Q_n(\mu) := \lambda^{-n} P_n(\mu)$ the *damped Legendre polynomials* ($Q_0 \equiv 1$, $Q_{-1} \equiv 0$). In the non–dissipative case ($\alpha_b = 0$) we have $|\lambda| = 1$, $\mu \in [-1,1]$, and hence $|P_n(\mu)| \leq 1$. In the dissipative case $\alpha_b > 0$ we have $|\lambda| > 1$, μ becomes complex and $|P_n(\mu)|$ typically grows with n. In order to evaluate ℓ_n in a numerically stable fashion it is therefore necessary to use the damped polynomials $Q_n(\mu)$ in (3.12).

The convolution coefficients (3.12) behave asymptotically as

$$\ell_n \cong -iH(-1)^n e^{in\xi}, \quad n \to \infty, \tag{3.13}$$

which may lead to subtractive cancellation in (3.11) (note that $\psi_J^m \approx \psi_J^{m+1}$ in a reasonable discretization). Therefore we use the following numerically more stable fashion of the DTBC in the implementation:

$$(1 + iq)\,\psi_{J-1}^n - \ell_0\,\psi_J^n = -(1 - iq)\,\psi_{J-1}^{n-1} + \sum_{m=1}^{n-1} \psi_J^m\, s_{n-m}, \tag{3.14}$$

with $s_n := \ell_n + e^{i\xi}\ell_{n-1}$, $n \geq 1$. The coefficients s_n are calculated as

$$s_n = \Big[(1 + iq)e^{i\xi} + \frac{i}{2}(\gamma - i\sigma)\Big]\delta_n^1 + \zeta\,\frac{Q_n(\mu) - \lambda^{-2}Q_{n-2}(\mu)}{2n - 1}. \tag{3.15}$$

Alternatively, they can be calculated directly with the recurrence formula

$$s_n = \frac{2n - 3}{n}\mu\lambda^{-1}s_{n-1} - \frac{n - 3}{n}\lambda^{-2}s_{n-2}, \quad n \geq 4, \tag{3.16}$$

once s_1, s_2, s_3 are computed from (3.15). Using asymptotic properties of the Legendre polynomials [42] one finds $s_n = O(n^{-3/2})$, $n \to \infty$ which agrees with the decay of the convolution kernel in the differential TBCs (2.10), (2.17).

This decay of the s_n motivates considering also a simplified version of the DTBC (3.14) with the convolution coefficients being cut off beyond an index M. This means that only the "recent past" (i.e. M range levels) is taken into account in the convolution in (3.14):

$$(1 + iq)\,\psi_{J-1}^n - \ell_0\,\psi_J^n = -(1 - iq)\,\psi_{J-1}^{n-1} + \sum_{m=n-M}^{n-1} \psi_J^m\, s_{n-m}. \tag{3.17}$$

This, of course, reduces the perfect accuracy of the DTBC (3.14), but it is numerically cheaper while still yielding reasonable results for moderate values of M. We remark that the resulting scheme does not conserve the discrete L^2–norm (cp. (3.2)), and hence the numerically stability of the simplified DTBC is not yet known.

So far we did not consider the (typical) density jump at the sea bottom in the DTBC (3.11). In the following we review two possible discretizations of the water–bottom interface. For the usual grid z_j, $j \in \mathbb{N}_0$ with $Jh = z_b$ the discontinuity of ρ is located at the grid point z_J. In this case it is a standard

practice [3, 34] to use (3.1) with

$$\rho_j = \begin{cases} \rho_w, & j < J, \\ \frac{2\,\rho_b\rho_w}{\rho_b+\rho_w}, & j = J, \\ \rho_b, & j > J. \end{cases} \tag{3.18}$$

As an alternative one may use an offset grid, i.e. $\tilde{z}_j = (j + \frac{1}{2})h$, $\tilde{\psi}_j^n \sim \psi(\tilde{z}_j, r_n)$, $j = -1(1)J$, where the water–bottom interface with the density jump lies between the grid points $j = J - 1$ and J. For discretizing the matching conditions in this case one wants to find suitable approximations for ψ and ρ at the interface z_b, $\Psi \sim \psi(z_b)$ and $\rho_{eff} = \rho(z_b)$, such that both sides of the discretized second matching condition (2.2b)

$$\frac{1}{\rho_w}\,\frac{\tilde{\psi}_J^n - \Psi}{h/2} = \frac{1}{\rho_b}\,\frac{\Psi - \tilde{\psi}_{J-1}^n}{h/2} \quad \text{are equal to} \quad \frac{1}{\rho_{eff}}\,\frac{\tilde{\psi}_J^n - \tilde{\psi}_{J-1}^n}{h}\,. \tag{3.19}$$

This approach results in an *effective density* $\rho_{eff} = (\rho_w + \rho_b)/2$ (based on a different derivation this was also used in [13]). In numerical tests we found that the offset grid with the above choice of ρ_{eff} produces slightly better results that have less Gibbs' oscillations at the discontinuity of ψ_z at z_b. This may be understood by the fact that (3.18) requires a higher order derivation (using the evolution equation) than our derivation (3.19) (see also [13, 29, 34]). Because of the discontinuity of ψ_z the higher order derivation yields (slightly) poorer results. Therefore we choose the offset grid for the implementation of the DTBC. At the surface we use instead of $\psi_0^n = 0$ the offset BC $\tilde{\psi}_0^n = -\tilde{\psi}_{-1}^n$.

Finally it remains to reformulate the DTBC (3.11) such that the density jump is taken into account. We rewrite the discretization of the second depth derivative at $j = J$ from (3.1):

$$h^2\left[\rho_J\,D_{\frac{h}{2}}^0\left(\rho_J^{-1}D_{\frac{h}{2}}^0\tilde{\psi}_J^n\right)\right] = \Delta_h^2\tilde{\psi}_J^n + \left(1 - \frac{\rho_b}{\rho_{eff}}\right)\left(\tilde{\psi}_J^n - \tilde{\psi}_{J-1}^n\right). \tag{3.20}$$

Comparing the r.h.s. of (3.20) to (3.6) we observe that only one additional term appears, and instead of (3.8) we get

$$\hat{\tilde{\psi}}_{J+1}(z) - \left[1 - iR\,\frac{\delta_b(z-1) - i\kappa_b(z+1)}{z+1+iq(z-1)}\right]\hat{\tilde{\psi}}_J(z) = \frac{\rho_b}{\rho_{eff}}\left(\hat{\tilde{\psi}}_J(z) - \hat{\tilde{\psi}}_{J-1}(z)\right). \tag{3.21}$$

Using $\hat{\tilde{\psi}}_{J+1}(z) = \nu_1(z)\,\hat{\tilde{\psi}}_J(z)$, where $\nu_1(z)$ denotes the solution of (3.9), and considering the fact that $\nu_1(z) + \nu_1^{-1}(z)$ is equal to the term in the squared brackets in (3.21) we obtain the Z–transformed DTBC:

$$\hat{\tilde{\psi}}_J(z) - \hat{\tilde{\psi}}_{J-1}(z) = \frac{\rho_{eff}}{\rho_b}\,\hat{\tilde{\psi}}_J(z) - \frac{\rho_{eff}}{\rho_b}\,\nu_1^{-1}(z)\hat{\tilde{\psi}}_J(z). \tag{3.22}$$

15

Hence, the DTBC including the density jump reads

$$(1 + iq)\frac{\rho_b}{\rho_{eff}}\,\tilde{\psi}_{J-1}^n + \left[(1 + iq)\left(1 - \frac{\rho_b}{\rho_{eff}}\right) - \ell_0\right]\tilde{\psi}_J^n$$

$$= -(1 - iq)\frac{\rho_b}{\rho_{eff}}\,\tilde{\psi}_{J-1}^{n-1} - (1 - iq)\left(1 - \frac{\rho_b}{\rho_{eff}}\right)\tilde{\psi}_J^{n-1} + \sum_{m=1}^{n-1}\tilde{\psi}_J^m\,s_{n-m}, \quad (3.23)$$

with the convolution coefficients s_n given by (3.15).

At the end of this Section we now address the question of *nonuniform depth discretizations*. In the derivation of the DTBC we needed a uniform z–discretization for the exterior problem on $z > z_b$, i.e. $j \geq J - 1$. For the interior problem, however, a nonuniform discretization (even adaptive in r) may be used, and this would not change our DTBC (3.23). For any given interior z–discretization and a uniform grid spacing h_b in the exterior domain, the DTBC will always yield, on the interior domain, the same solution as the corresponding discrete half–space solution.

This raises a natural question: given an interior (possibly nonuniform) z–discretization, what is the best uniform discretization of the exterior domain? To analyze this question we first consider the three types of errors that are relevant here: Firstly, the error associated with the given interior discretization does not depend on the choice of h_b. In order to avoid strong reflections due to the nonuniform grid we will assume that the interior grid spacing $h_j := z_j - z_{j-1}$ "varies slowly with j" and can be represented as $h_j = h(z_j)$ with a "smooth" function $h(z)$. To the authors' knowledge, the reflections in irregular grids have not yet been theoretically analyzed for the Schrödinger equation, but very similar effects appear in hyperbolic and parabolic equations [46, 32]. In numerical tests, however, one can easily verify that discontinuities of $h(z)$ would introduce spurious numerical reflections of an incident wave (cp. [46] and references therein). Such reflections can be largely reduced by "smoothing" such a discontinuity of $h(z)$ (cf. Example 4 of §4).

Secondly, the discrete BC at z_b may cause outgoing waves to be partially reflected back into the computational domain, and these reflections strongly depend on h_b.

Finally, for the discretization error of the (uniformly discretized) exterior domain we have to distinguish between traveling waves and evanescent waves. In the first case the discretization error can be interpreted as a modification to the dispersion relation for the outgoing waves (incoming waves are not present in the exterior domain). But the accuracy of their propagation speed is irrelevant, as long as we are only interested in the solution in the interior domain. Hence, the exterior discretization error can be disregarded for outgoing traveling waves. The discretization error of evanescent waves, however, influences the interior solution.

Since our DTBC is fully equivalent to a discrete half–space problem, the above discussion of the three error types can be completly reduced to the problem of *internal grid reflections* for the SPE or the WAPE. In the continuous limit ($h_b \to 0$) of the exterior discretization, this also holds for the semi–discrete approach of [39, 40] for the Schrödinger equation. Following the

16

above discussion we can now give the best exterior discretization in the 'traveling wave regime': the uniform exterior grid spacing $h_b = h(z_b)$ generates a completely reflection–free BC and the uniformity of the exterior grid ensures that the outgoing waves will never be reflected back. Their inaccurate resolution in the exterior domain only causes inaccurate wave speeds, but this does not affect the interior solution.

This behaviour is numerically verified in the simulations of §5 in [40], where a uniformly spaced grid was compared to the semi–discrete approach for the exterior domain. There, a Schrödinger equation with a constant potential is considered, and hence the initial Gaussian wave packet consists only of traveling wave modes in the exterior domain.

In the 'evanescent wave regime', however, the picture is not that simple, and it is not known yet whether there exists a exists a unique 'best exterior discretization'. Our simulations of §4 indicate that it may indeed be advantageous to use a DTBC that corresponds to a finer exterior discretization, as long as the interior and exterior grid spacings are gradually matched to each other.

4. Numerical Examples

In the first two examples of this Section we shall consider the SPE and the WAPE for comparing the numerical result from using our new discrete TBC to the solution using either the discretized TBC of Thomson and Mayfield [45] or an absorbing layer. Due to its construction, our DTBC yields exactly (up to round–off errors) the numerical half–space solution restricted to the computational interval $[0, z_b]$. The simulation with discretized TBCs requires the same numerical effort. However, their solution may (on coarse grids) strongly deviate from the half–space solution.

In each example we used the Gaussian beam from [28] as initial data. Below we present the transmission loss $-10 \log_{10} |p|^2$, where the acoustic pressure p is calculated from (1.3).

Example 1. This is a well–known benchmark problem from the literature [28, 37, 45]. In this example the ocean region $(0 < z < 240\,\text{m})$ with the uniform density $\rho_w = 1.0\,\text{gcm}^{-3}$ is modeled by the SPE (1.6). It contains no attenuation and a large density jump $(\rho_b = 2.1\,\text{gcm}^{-3})$ at the water–bottom interface. Hence, this problem provides a test of the treatment of the density jump in the TBCs applied along $z_b = 240\,\text{m}$.

The source of $f = 100\,\text{Hz}$ is located at a water depth $z_s = 30\,\text{m}$ and the receiver depth is at $z_r = 90\,\text{m}$. The sound speed profile in water is given by $c(z) = 1498 + |120 - z|/60\,\text{ms}^{-1}$, and the sound speed in the bottom is $c_b = 1505\,\text{ms}^{-1}$. For our calculations up to a maximum range of 20 km we used a reference sound speed $c_0 = 1500\,\text{ms}^{-1}$ and a uniform computational grid with depth step $\Delta z = 2\,\text{m}$ and range step $\Delta r = 5\,\text{m}$ (the same step sizes were used in [45]).

In Figure 1 the solid line is the solution with our new discrete TBC (3.23) and the dotted line is obtained with the discretized TBC (3.3). The discretized

TBC clearly introduces a systematic phase–shift error, which is roughly proportional to Δz. The discretized TBC also produces artificial oscillations (cf. the zoomed region), while our new DTBC yields the smooth solution with the same numerical effort.
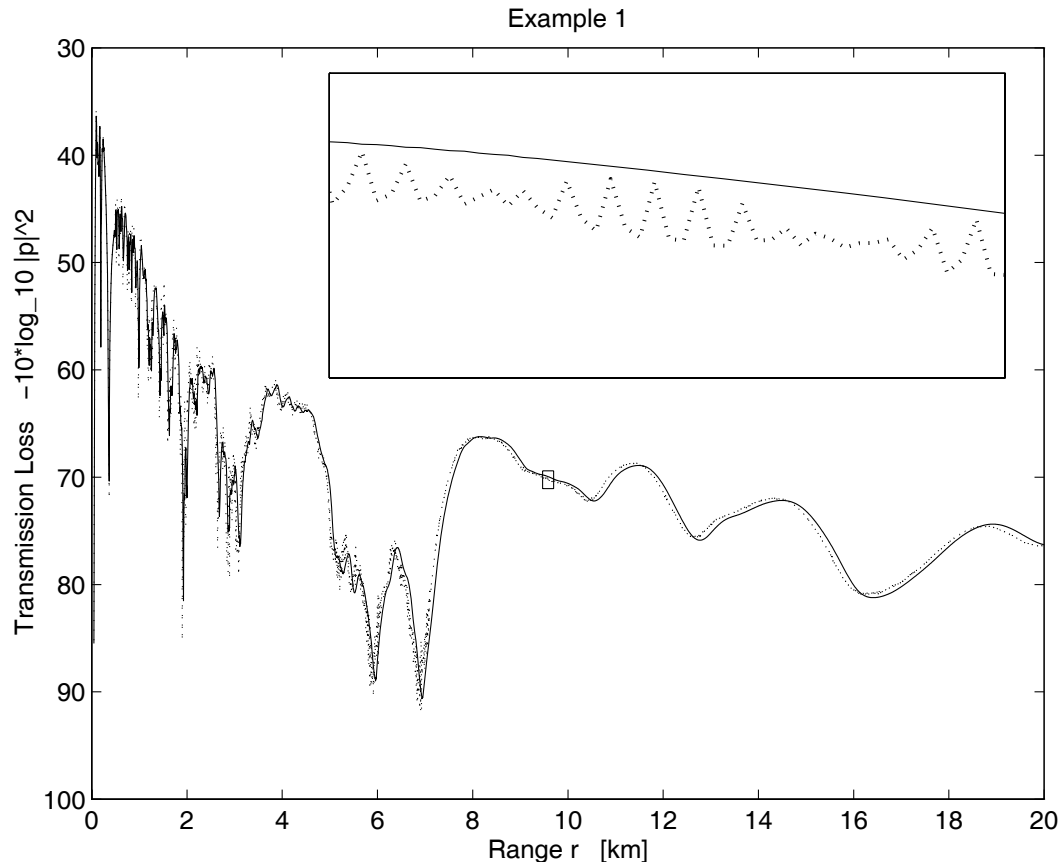

FIGURE 1. Transmission loss at $z_r = 90\,\mathrm{m}$ for Example 1: the solution with the new discrete TBC (—) coincides with the half–space solution, while the solution with the discretized TBC ($\cdots$) introduces a phase–shift and artificial oscillations.

Figure 2 compares the results of our new discrete TBC (solid line) to the solution obtained with an absorbing layer of $240\,\mathrm{m}$ thickness (dotted line) and a homogeneous Dirichlet BC at $z_{max} = 480\,\mathrm{m}$. Hence the computation took about twice as long as by using the discrete TBC. In our experiments we obtained a better match to the 'exact' half-space solution by using the *exponential absorption profile*

$$\alpha_b(z) = 10\left[\exp\left\{4\,\frac{z - z_b}{z_{max} - z_b}\right\} - 1\right] \mathrm{dB}\,/\lambda_b, \quad z_b < z < z_{max}, \tag{4.1}$$

rather than a linear profile. We remark that the profile (4.1) and thickness of the absorbing layer were designed as to yield a close match to the 'correct' solution. Without such an 'a–posteriori data fitting', however, a calculation with an absorbing layer would usually yield a solution with a somewhat larger deviation than suggested by Figure 2. With a thicker layer one can of course
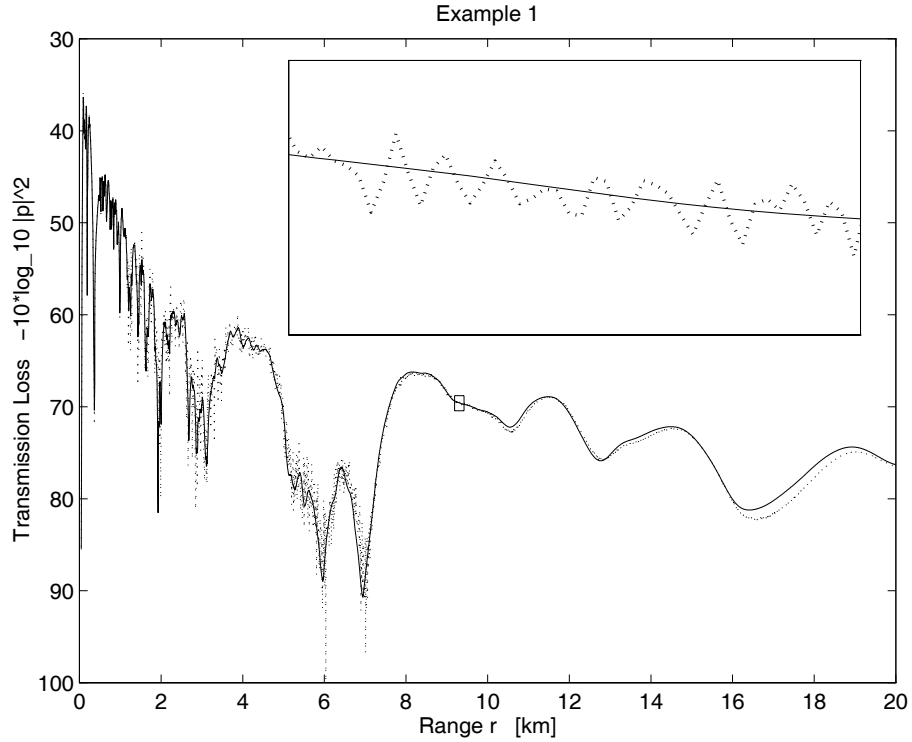
FIGURE 2. Transmission loss at $z_r = 90\,\mathrm{m}$ for Example 1: the solution with an absorbing layer of $240\,\mathrm{m}$ ($\cdots$) is quite satisfactory in comparison to the 'exact' solution computed with the discrete TBC (—). It is in phase but shows some artificial oscillations and overestimates the transmission loss at 6km, 7km, and in the range 16–19km.

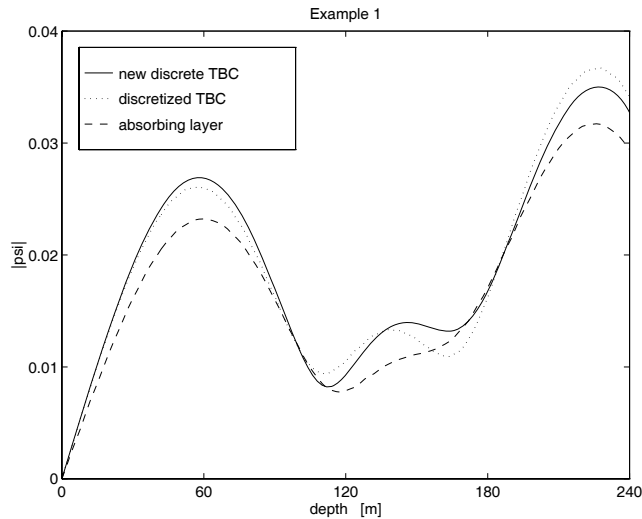still improve the results of Figure 2, e.g. no more artificial oscillations are visible when using a layer of $760\,\mathrm{m}$.

FIGURE 3. Vertical cut of the 3 solutions at $r = 19\,\mathrm{km}$ for Example 1: $|\psi(z, r = 19\,\mathrm{km})|$

Figure 3 shows the significant deviations of the solutions using either the discretized TBC or an absorbing layer of 240 m from the computed half–space solution, which coincides with the solution using our new DTBC.

Example 2. This example appeared as the NORDA test case 3B in the PE Workshop I [26, 28, 37, 45]. The environment for this example consists of an isovelocity water column ($c(z) = 1500\,\mathrm{ms}^{-1}$) over an isovelocity half–space bottom ($c_b = 1590\,\mathrm{ms}^{-1}$). The density changes at $z_b = 100\,\mathrm{m}$ from $\rho_w = 1.0\,\mathrm{gcm}^{-3}$ in the water to $\rho_b = 1.2\,\mathrm{gcm}^{-3}$ in the bottom. The source and the receiver are located at the same depth near the bottom: $z_s = z_r = 99.5\,\mathrm{m}$. The source frequency is $f = 250\,\mathrm{Hz}$. The attenuation in the water is zero, and the bottom attenuation is $\alpha_b = 0.5\,\mathrm{dB}\,/\lambda_b$, where $\lambda_b = c_b/f$ denotes the wavelength of sound in the bottom. Here, the steepest angle of propagation (which is the equivalent ray–angle of the highest of the 11 propagating modes) is approximately $20°$ (cf. [26, 45]). Since the source is located near the bottom, the higher modes are significantly excited. Therefore the wide angle capability is important here and we use the WAPE (1.8) (with the coefficients of Claerbout) to solve this benchmark problem.

The maximum range of interest is 10 km and the reference sound speed is chosen as $c_0 = 1500\,\mathrm{ms}^{-1}$. The calculations were carried out using the depth step $\Delta z = 0.25\,\mathrm{m}$ and the range step $\Delta r = 2.5\,\mathrm{m}$. Since the source is placed close to the bottom, the TBC was applied 10 m below the ocean–bottom interface
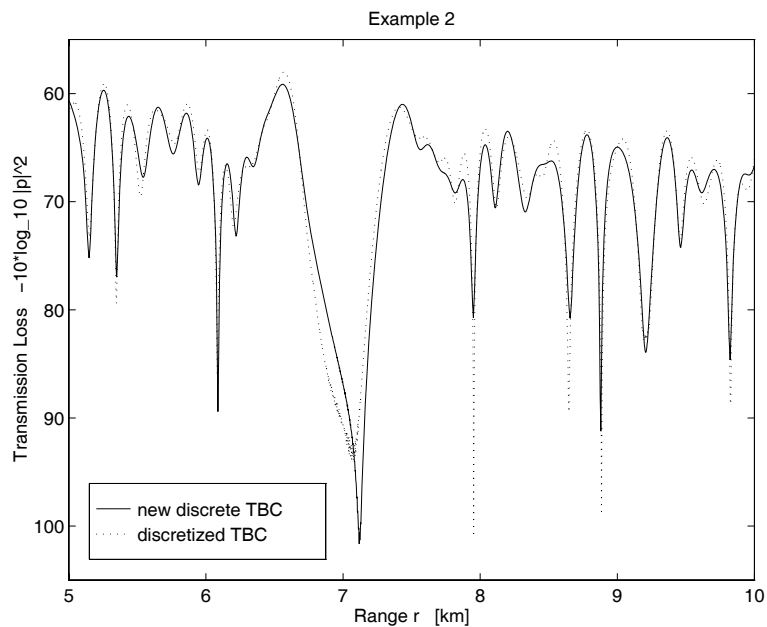

FIGURE 4. Transmission loss at $z_r = 99.5\,\mathrm{m}$ for Example 2: the solution with the new discrete TBC coincides with the half–space solution, while the solution with the discretized TBC still deviates significantly from it for the chosen discretization.

The typical feature of this problem is the large destructive interference null at a range of 7 km. Figure 4 compares the transmission loss results for the discrete and discretized TBCs in the range from 5 to 10 km. In a second comparison we extended the computational domain up to 200 m. With the given

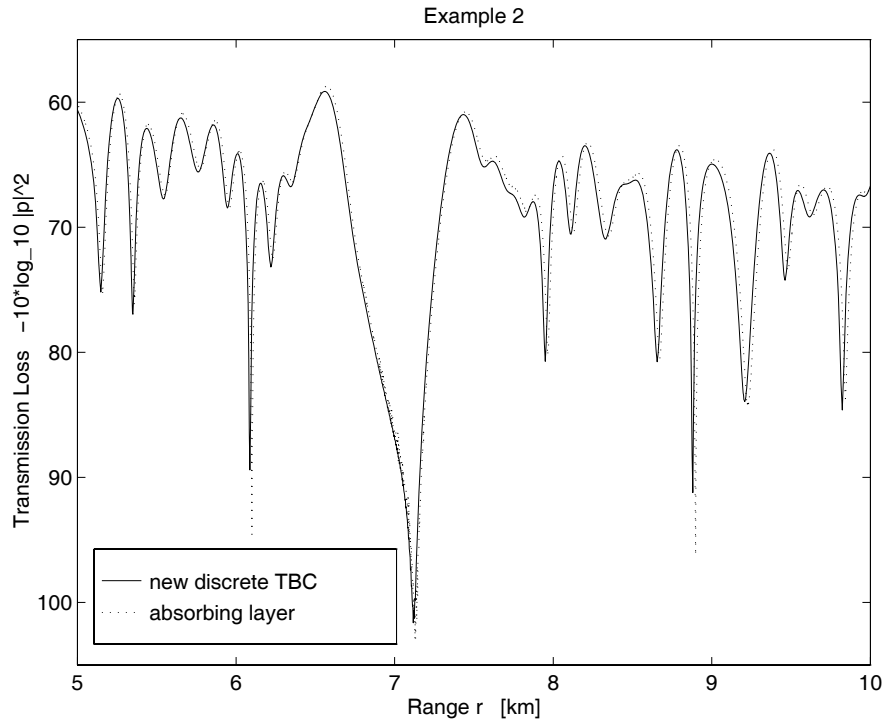bottom attenuation this 100 m layer is thick enough to yield the reasonable approximation shown in Figure 5.

Example 2

FIGURE 5.   Transmission loss at $z_r = 99.5\,\mathrm{m}$ for Example 2: in comparison to the exact half–space solution, the truncation of the computational domain at 200 m (the given bottom attenuation then represents an absorbing layer of 100 m) introduces a slight phase shift.

Figure 6 shows the deviation of the solutions with the discretized TBC and with the absorbing layer from the computed half–space solution, which coincides with the solution using our new discrete TBC.

Example 3. In this example we illustrate the theoretical findings of §2 on coupled models. We use the physical parameters of the first two examples but different models for the water and the bottom region.

We start with considering the environment of Example 2 and compare the results of different model couplings. First we fix the WAPE of Claerbout (CWAPE; $p_0 = 1$, $p_1 = \frac{3}{4}$, $q_1 = \frac{1}{4}$) in the bottom and choose a different (and in fact better) rational approximation (GWAPE) for the water region that fulfills the coupling condition (2.23): $p_1 = 3\,q_1$. The two remaining parameters p_0, q_1 are then determined by minimizing the approximation error of $(1 - \lambda)^{\frac{1}{2}}$ (in the maximum norm) over the interval $[0.0008, 0.103]$, which contains the discrete spectrum of L: $p_0 = 1.0000071$, $q_1 = 0.2501753$. We compare this approximation to the case of also using the CWAPE in the water. Furthermore, we show the results when using the SPE in the sea bottom (which clearly violates (2.23)) and when using the SPE in both regions.
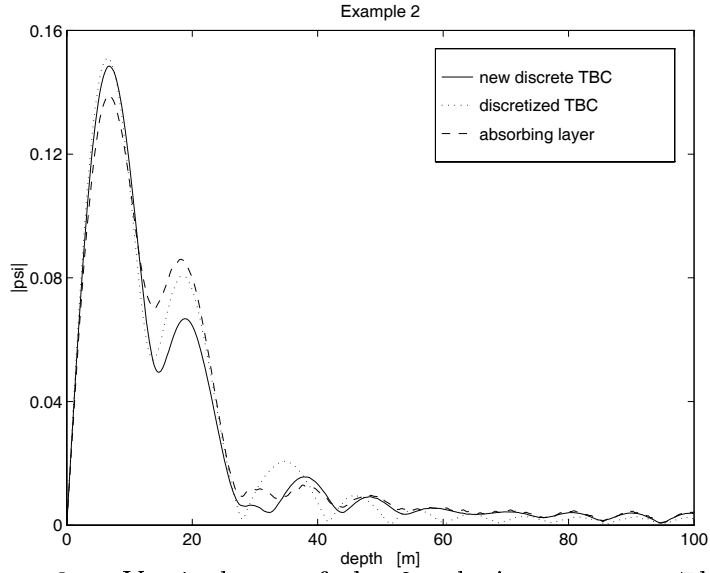
21

FIGURE 6. Vertical cut of the 3 solutions at $r = 7\,\mathrm{km}$ for Example 2: $|\psi(z, r = 7\,\mathrm{km})|$
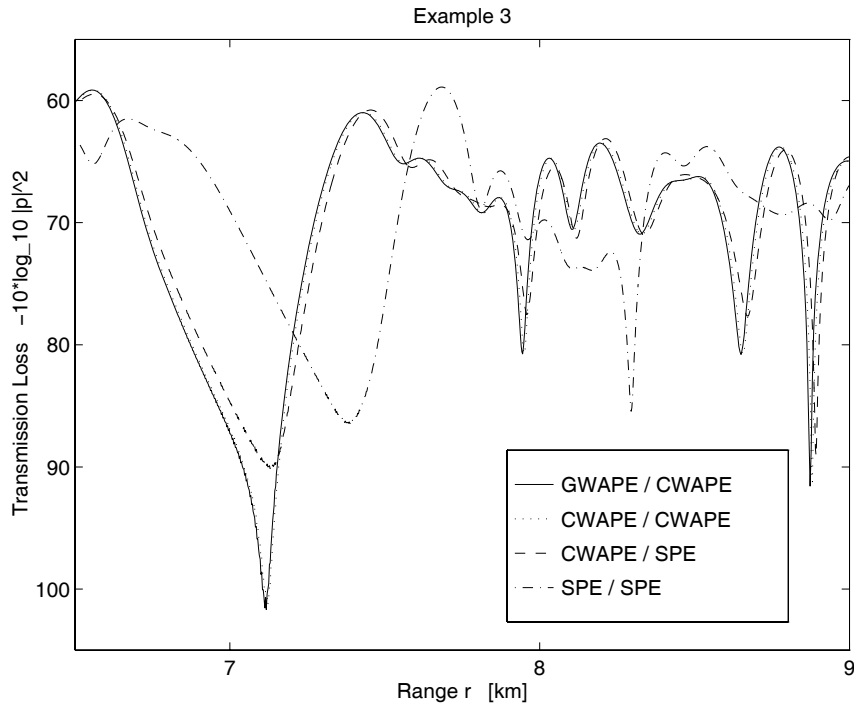

FIGURE 7. Transmission loss at $z_r = 99.5\,\mathrm{m}$ in several coupled models (water and sea bottom) for the simulation of Example 2.

Figure 7 displays a comparison of the transmission loss from 6.5 to 9 km for these different couplings. It turns out that the solution for the coupled GWAPE/CWAPE model is very close to the one using the CWAPE in both media. While the CWAPE/SPE model violates the coupling condition, it only

22

deviates from the above solutions by a slight phase–shift that is typical for the SPE in this example (cp. also the "pure" SPE model).

Now we turn to the dissipation–free situation of Example 1 and focus our attention on a conservative discretization of coupled models that satisfy the coupling condition $p_1(z)/q_1(z) = \mu = $ const, and hence preserve the $L^2(\mathbb{R}^+; (\sigma\rho)^{-1}dz)$–norm (see §2). As a discrete analogue of (2.6) we obtain in the dissipation–free case

$$hD_k^+ \sum_{j=0}^{J-1} \frac{\left|\tilde{\psi}_j^n\right|^2}{\sigma\tilde{\rho}_j} = -\frac{2}{p_1^2 k_0 \rho_{eff}} \mathrm{Im}\left[\overline{\left((p_1 - q_1)\tilde{\psi}_{J-1}^{n+\frac{1}{2}} + iq_1 k_0^{-1} D_k^+ \tilde{\psi}_{J-1}^n\right)} \times \right.$$
$$\left. \times \left((p_1 - q_1)D_h^+ \tilde{\psi}_{J-1}^{n+\frac{1}{2}} + iq_1 k_0^{-1} D_k^+ D_h^+ \tilde{\psi}_{J-1}^n\right)\right], \quad (4.2)$$

with $\tilde{\rho}_j = \rho(\tilde{z}_j)$ and $\sigma = p_1^2/(p_1 - p_0 q_1)$. Analogously, a discrete version of (2.7) can be shown for the bottom region $j \geq J$:

$$hD_k^+ \sum_{j=J}^{\infty} \frac{\left|\tilde{\psi}_j^n\right|^2}{\sigma_b\rho_b} = \frac{2}{(p_1^b)^2 k_0 \rho_{eff}} \mathrm{Im}\left[\overline{\left((p_1^b - q_1^b)\tilde{\psi}_{J-1}^{n+\frac{1}{2}} + iq_1^b k_0^{-1} D_k^+ \tilde{\psi}_{J-1}^n\right)} \times \right.$$
$$\left. \times \left((p_1^b - q_1^b)D_h^+ \tilde{\psi}_{J-1}^{n+\frac{1}{2}} + iq_1^b k_0^{-1} D_k^+ D_h^+ \tilde{\psi}_{J-1}^n\right)\right], \quad (4.3)$$

with $\sigma_b = (p_1^b)^2/(p_1^b - p_0^b q_1^b)$. For coupled models σ usually takes different values in the water and bottom regions. It follows from (4.2), (4.3) that the weighted discrete L^2–norm on $j \in \mathbb{N}_0$ is preserved:

$$\|\tilde{\psi}^n\|^2 = h\sum_{j=0}^{J-1} \frac{\left|\tilde{\psi}_j^n\right|^2}{\sigma\tilde{\rho}_j} + h\sum_{j=J}^{\infty} \frac{\left|\tilde{\psi}_j^n\right|^2}{\sigma_b\rho_b} = \mathrm{const} \quad (4.4)$$

provided that the coupling condition (2.23) is fulfilled.

Figure 8 illustrates that the discrete L^2–norm (4.4) is conserved as long as the coupling condition (2.23) is satisfied. In all four simulations we used the WAPE of Claerbout for the water region and different models in the sea bottom: only the hybrid WAPE–model with constant $p_1(z)/q_1(z) = \mu = 3$ renders the scheme conservative (only for this numerical illustration we choose the values $p_0 = 0.6$, $q_1 = 0.2$). A coupling to the SPE (like in [37]) or to a WAPE in the bottom with $p_1^b/q_1^b = \mu_b \neq 3$ all yields a non–conservative scheme. We point out that these schemes are not only non–conservative for the particular norm (4.4) but also for any other weighted L^2–norm.

In the simulations for Figure 8, the second sum of (4.4) (for the exterior of the computational domain) was evaluated via (4.3).

Example 4. In this example we illustrate our discussion from §3 on the 'best uniform exterior discretization' for the case of evanescent waves. We want to answer the following question: given a uniform interior discretization, can the result from a globally uniform z–discretization be improved by choosing a finer exterior z–discretization, or, equivalently, by using a DTBC that corresponds to such a finer discretization?
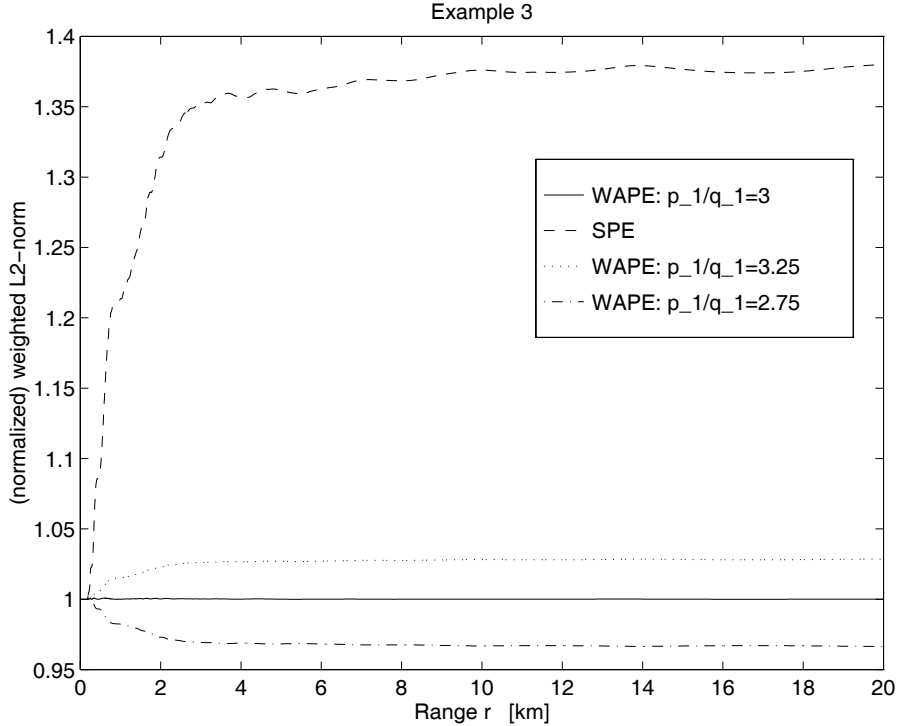
FIGURE 8. Coupled WAPE–models conserve the discrete L^2–norm (4.4) only when satisfying the coupling condition $p_1/q_1 = \mu = \text{const}$ (—).

As a model problem for this test we consider the SPE (1.6) on $z > 0$, $r > 0$ with a homogeneous Dirichlet BC at $z = 0$, $k_0 = 2\,\text{m}^{-1}$ and the "potential well" $V(z) = 0$, $0 < z < z_b = 100\,\text{m}$, $V(z) = V_b = 0.3$, $z > z_b$. In this example, plane waves with a wave number $k < k_{crit} = \sqrt{1.2}\,\text{m}^{-1}$ are evanescent in the exterior domain $z > z_b$, and $k > k_{crit}$ transmits a traveling wave into the exterior. We choose here the Gaussian beam $\exp(ikz - 0.003\,\text{m}^{-2}(z - 50\,\text{m})^2)$ with $k = 1\,\text{m}^{-1}$ as an initial condition. For this choice of k 'most' of the Fourier components of this wave correspond to evanescent modes in the bottom. Hence, this wave will be predominantly reflected back into the interior domain.

Figure 9 compares the effect of choosing different (uniform and nonuniform) z–discretizations. We show the results of this simulation at the range $r = 200\,\text{m}$ when the wave packet has been reflected back from the water–bottom interface. The solid line was obtained with the uniform z–discretization $h_0 = 0.05\,\text{m}$, and it will serve as our 'exact' reference solution. The dashed line shows the solution with the uniform grid spacing $h_1 = 0.25\,\text{m}$. In the following comparisons we will keep this coarser interior grid and will vary the uniform exterior grid. Following our discussion from §3, we used a gradual transition between these two grid spacings in the depth interval $100 - 110\,\text{m}$ (piecewise linear grid spacing function $h(z)$).

The dotted curve of Figure 9 gives the results with the finer exterior z–discretization $h_2 = 0.1\,\text{m}$. Close to the sea bottom it shows significant improvements over the uniform discretization with h_1. In the interval $0 < z < 60\,\text{m}$
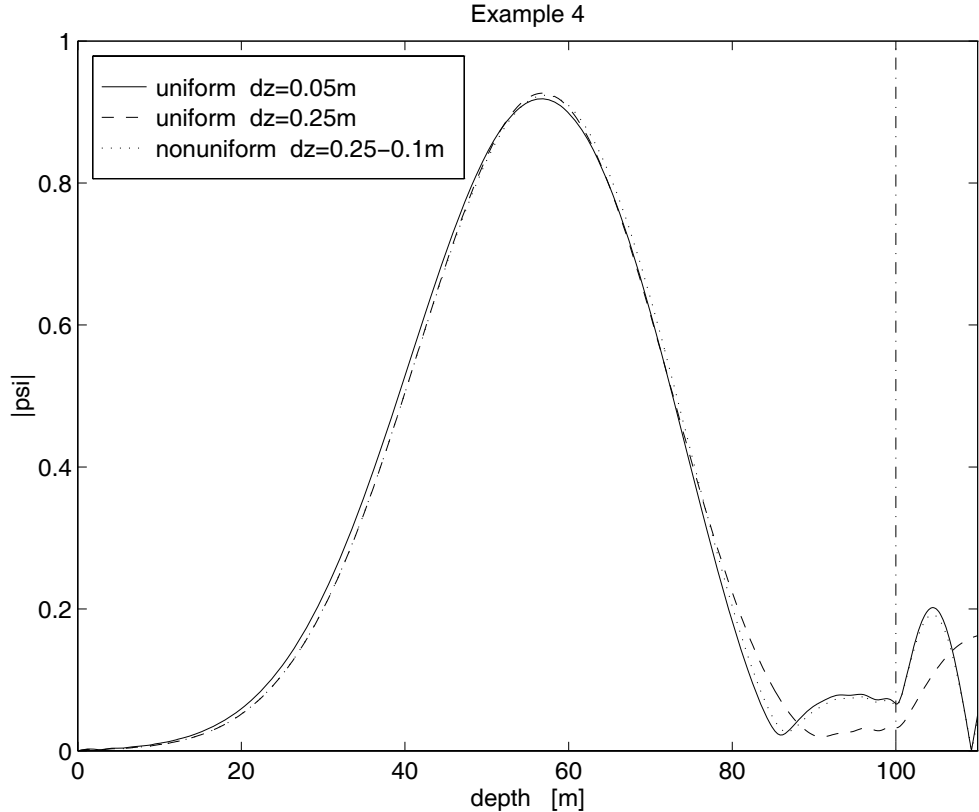
FIGURE 9. The 'best uniform exterior z–discretization' may be finer than the interior discretization. Vertical cut of the three solutions at $r = 200\,\mathrm{m}$ for Example 4: the solution $(\cdots)$ calculated on a nonuniform grid (finer grid in the exterior domain than in the interior) is more accurate in the interior domain than the solution obtained on a uniformly coarse grid $(---)$. The reference solution (—) was calculated on a uniformly fine grid.

both curves almost coincide as the interior discretization error is dominant there, and it implies inaccurate wave speeds that are reflected in the clearly visible phase shift. The dotted curve still exhibits this phase shift up to the sea bottom at $100\,\mathrm{m}$, but for the dashed curve the error in the interval $80\,\mathrm{m} < z < 100\,\mathrm{m}$ is dominated by the effect of the exterior discretization. It thus seems that the effect of the reduced exterior discretization error (due to the finer exterior discretization) may outweigh (in the interior domain!) the additional reflection errors incurred by the nonuniform grid.

The $L^2(0, 100)$–errors (w.r.t. the solid curve) of the solutions with the uniform h_1–discretization and the nonuniform $h_1\,/\,h_2$–discretization are, respectively, 0.0370 and 0.0267. Using an even finer exterior discretization does not seem to improve the result much further (L^2–error 0.0266 for the $h_1\,/\,h_0$–discretization). A finer exterior discretization would, however, require a thicker region to adapt the two grids.

We thus conclude that finer exterior discretizations may indeed be advantageous in the case of evanescent waves, and for large ranges these are the important modes in the considered applications of underwater acoustics.

5. CONCLUSIONS

We have derived a new discretization (*discrete TBC*) of the TBC for the WAPE of acoustics. It is of discrete convolution form involving the boundary data from the whole "past range". The convolution coefficients s_n are calculated via a simple three–term recurrence relation and they decay like $O(n^{-3/2})$. Since our new DTBC has the same convolution structure as existing discretizations, it requires the same computational effort but improves two shortcomings: DTBCs are more accurate (in fact, as accurate as the discrete half–space problem) and they yield an unconditionally stable scheme.

We point out that the superiority of DTBCs over other discretizations of TBCs is not restricted to the WAPE or to our particular interior discretization scheme (see e.g. [5, 17, 19]). The crucial point of our derivation was to find the inverse Z–transformation of (3.10) explicitly. In more general applications (e.g. higher order Padé approximations or 3D–problems) it might be necessary to derive the convolution coefficients in (3.14) through a numerical inverse Z–transformation [30], but this does not change the efficiency and stability of the presented method. As a general philosophy, DTBCs should be used whenever highly accurate solutions are important.

APPENDIX A. PROOF OF THEOREM 1
(WELL–POSEDNESS OF THE WAPE)

In Theorem 1 we assumed that V, ρ, $\rho^{-1} \in L^\infty(\mathbb{R}^+)$. Then, the Schrödinger operator

$$L = -k_0^{-2} \rho \, \partial_z (\rho^{-1} \partial_z) + V(z) \tag{A.1}$$

with a homogeneous Dirichlet BC at $z = 0$ is self–adjoint in $L^2(\mathbb{R}^+; \rho^{-1} dz)$ with the dense domain

$$D(L) = H_0^1(\mathbb{R}^+) \cap \left\{ \varphi | \rho^{-1} \varphi_z \in H^1(\mathbb{R}^+) \right\}. \tag{A.2}$$

We now consider the operator $f(L) = \frac{p_0 - p_1 L}{1 - q_1 L}$ defined as

$$f(L) = \int_{-\infty}^{\infty} f(\lambda) \, dP_\lambda, \tag{A.3}$$

with dP_λ denoting the projection valued spectral measure of the operator L (cf. [18, 38]). According to [18, Th. XII.2.6] the domain of $f(L)$ is dense in $L^2(\mathbb{R}^+; \rho^{-1} dz)$ if and only if $\tilde{\lambda} = q_1^{-1}$, the pole of $f(\lambda)$, is not an eigenvalue of L. In this case $f(L)$ is self–adjoint and, by Stone's Theorem [38], $ik_0 f(L)$ generates a unitary C_0–group on $L^2(\mathbb{R}^+; \rho^{-1} dz)$, which yields the unique solution to (2.1). $\qquad \square$

If $\tilde{\lambda}$ coincides with an eigenvalue λ_j of L, then (2.1) still admits a unique mild solution for all initial data in the orthogonal complement of φ_j, the unique eigenfunction corresponding to λ_j. Theorem 1 generalizes the well–posedness analysis for the WAPE on finite intervals given in [3]. There, however, $\tilde{\lambda}$ can easily lie in the (pure eigenvalue) spectrum of L, what then restricts the class of admissible initial conditions.

Appendix B. WAPE–SPE coupling

Here, we discuss the mathematically sound formulation of the coupled WAPE–SPE model for the simple model case of constant c and ρ. We first consider the pseudo–differential operator $f(L)$ appearing in the WAPE (2.1) with $L = -k_0^{-2}\partial_z^2$. Due to the BC at $z = 0$ it can be expressed in terms of Fourier–sine transforms as

$$\big(f(L)\psi\big)(z) = \frac{2}{\pi} \int_0^\infty \int_0^\infty \Phi(\xi)\psi(y)\sin(\xi y)\sin(\xi z)\,dy\,d\xi, \tag{B.1}$$

with the symbol

$$\Phi(\xi) = \frac{p_0 - p_1 k_0^{-2}\xi^2}{1 - q_1 k_0^{-2}\xi^2}. \tag{B.2}$$

In the coupled WAPE–SPE model one would formally want to write the evolution equation as

$$\psi_r = ik_0 A\psi \tag{B.3}$$

with

$$A\psi = \begin{cases} \left(\dfrac{p_0 + p_1 k_0^{-2}\partial_z^2}{1 + q_1 k_0^{-2}\partial_z^2} - 1\right)\psi, & 0 < z < z_b, & \text{(B.4a)} \\ \dfrac{k_0^{-2}}{2}\partial_z^2\psi, & z > z_b. & \text{(B.4b)} \end{cases}$$

However, as the pseudo–differential operator in (B.4a) is non–local, acting on $L^2(\mathbb{R}^+)$, it cannot be simply restricted to the interval $0 < z < z_b$. It is therefore appropriate to define the coupled evolution equation on the symbol level of the two involved operators (cf. [20, 25]). Without attenuation both the SPE and the WAPE conserve the L^2–norm and the discrete analogue of this conservation is the main ingredient for showing unconditional stability of the finite difference scheme in §3. Therefore we postulate that the coupled model also has to conserve the L^2–norm. This can be achieved if the operator A on the right hand side of (B.3) is interpreted as the Weyl operator (see [20])

$$A\psi(z) = \frac{2}{\pi}\int_0^\infty \int_0^\infty a\left(\frac{y+z}{2},\xi\right)\psi(y)\sin(\xi y)\sin(\xi z)\,dy\,dz \tag{B.5}$$

to the symbol

$$a(z,\xi) = \begin{cases} \Phi(\xi) - 1, & 0 < z < z_b, \\ -\frac{k_0^{-2}}{2}\xi^2, & z > z_b. \end{cases} \tag{B.6}$$

As $a(z,\xi)$ is real, one readily verifies that the evolution equation (B.3), (B.5) conserves the L^2–norm.

Due to the pole of the symbol $\Phi(\xi)$ it would be quite difficult to appropriately discretize (B.3), (B.5), and it is beyond our scope here. We remark that finite difference schemes of pseudo–differential equations with smooth symbols have recently been studied in [31].

ACKNOWLEDGEMENT

References

[1] M. Abramowitz and I.A. Stegun, *Handbook of Mathematical Functions*, National Bureau of Standards, Applied Math. Series #55, Dover Publications, 1965.

[2] D.S. Ahluwalia and J.B. Keller, *Exact and asymptotic representations of the sound field in a stratified ocean*, in *Wave Propagation and Underwater Acoustics*, Lecture Notes in Physics 70, eds. J.B. Keller and J.S. Papadakis, Springer, New York, 1977, pp. 14–85.

[3] G.D. Akrivis, V.A. Dougalis and G.E. Zouraris, *Error Estimates for Finite Difference Methods for a Wide–Angle "Parabolic" Equation*, SIAM J. Num. Anal. **33** (1996), 2488–2509.

[4] D.E. Amos, *Algorithm 644: A Portable Package for Bessel Functions of a Complex Argument and Nonnegative Order*, ACM Trans. Math. Software **12** (1986), 265–273; *Remark on Algorithm 644*, ACM Trans. Math. Software **16** (1990), 404; *A Remark on Algorithm 644*, ACM Trans. Math. Software **21** (1995), 388–393.

[5] A. Arnold, *Numerically Absorbing Boundary Conditions for Quantum Evolution Equations*, To appear in: *Proceedings of the "International Workshop on Computational Electronics"*, Tempe, USA, 1995; VLSI Design **6** (1998), 313–320.

[6] A. Bamberger, B. Engquist, L. Halpern and P. Joly, *Parabolic wave equation approximations in heterogeneous media*, SIAM J. Appl. Math. **48** (1988), 99–128.

[7] V.A. Baskakov and A.V. Popov, *Implementation of transparent boundaries for numerical solution of the Schrödinger equation*, Wave Motion **14** (1991), 123–128.

[8] *Bateman Manuscript Project*, Tables of Integral Transforms, vol. 1, McGraw–Hill, 1954.

[9] C.H. Bruneau and L. Di Menza, *Conditions aux limites transparentes et artificielles pour l'équation de Schrödinger en dimension 1 d'espace*, C. R. Acad. Sci. Paris, Ser. I **320** (1995), 89–94.

[10] J.F. Claerbout, *Coarse grid calculation of waves in inhomogeneous media with application to delineation of complicated seismic structure*, Geophysics **35** (1970), 407–418.

[11] J.F. Claerbout, *Fundamentals of Geophysical Data Processing*, McGraw–Hill, New York, 1976.

[12] M.D. Collins, *Applications and time–domain solution of higher–order parabolic equations in underwater acoustics*, J. Acoust. Soc. Am. **86** (1989), 1097–1102.

[13] M.D. Collins, *A higher–order parabolic equation for wave propagation in an ocean overlying an elastic bottom*, J. Acoust. Soc. Am. **86** (1989), 1459–1464.

[14] M.D. Collins, *Higher–Order and elastic parabolic equations for wave propagatiion in the ocean*, in *Computational Acoustics, vol. 3*, eds. D. Lee, A. Cakmak, and R. Vichnevetsky, Proceedings of IMACS, New Brunswick, NJ, 167–184, 1990.

[15] M.D. Collins, *A split–step Padé solution for the parabolic equation method*, J. Acoust. Soc. Am. **93** (1993), 1736–1742.

[16] L. Di Menza, *Approximations numériques d'équations de Schrödinger non linéaires et de modèles associés*, Ph.D. thesis, Université Bordeaux I, 1995.

[17] J. Douglas Jr., J.E. Santos, D. Sheen and L.S. Bennethum, *Frequency domain treatment of one–dimensional scalar waves*, Math. Mod. and Meth. in Appl. Sc. **3** (1993), 171–194.

[18] N. Dunford and J.T. Schwartz, *Linear Operators, Part II: Self Adjont Operators in Hilbert Space*, John Wiley Interscience Publishers, New York, 1963.

[19] M. Ehrhardt, *Discrete Tranparent Boundary Conditions for Parabolic Equations*, in *Proceedings of the GAMM 96 Conference*, ZAMM vol. 77, Supplement 2, S543-S544, 1997.

[20] L. Fishman, *Exact and operator rational approximate solutions of the Helmholtz, Weyl composition equation in underwater acoustics — The quadratic profile*, J. Math. Phys. **33** (1992), 1887–1914.

[21] R.R. Greene, *The rational approximation to the acoustic wave equation with bottom interaction*, J. Acoust. Soc. Am. **76** (1984), 1764–1773.

[22] R.R. Greene, *A high–angle one–way wave equation for seismic wave propagation along rough and sloping interfaces*, J. Acoust. Soc. Am. **77** (1985), 1991–1998.

[23] L. Halpern and L.N. Trefethen, *Wide–angle one–way wave equations*, J. Acoust. Soc. Amer. **84** (1988), 1397–1404.

[24] J.R. Hellums and W.R. Frensley, *Non–Markovian open–system boundary conditions for the time–dependent Schrödinger equation*, Phys. Rev. B **49** (1994), 2904–2906.

[25] L. Hörmander, *The analysis of linear partial differential operators III: Pseudo–differential operators*, Grundlehren der Mathematischen Wissenschaften 274, Springer–Verlag, Berlin, 1985.

[26] F.B. Jensen and W.A. Kuperman, *Consistency Tests of Acoustic Propagation Models*, SACLANTCEN Memorandum SM – **157**, 1982.

[27] J.E. Lagnese, *General boundary value problems for differential equations of Sobolev type*, SIAM J. Math. Anal. **3** (1972), 105–119.

[28] D. Lee and S.T. McDaniel, *Ocean acoustic propagation by finite difference methods*, Comput. Math. Appl. **14** (1987), 305–423.

[29] D. Lee, G. Botseas and J.S. Papadakis, *Finite–difference solution to the parabolic wave equation*, J. Acoust. Soc. Am. **70** (1981), 795–800.

[30] J.N. Lyness, *Algorithm 413: ENTCAF and ENTCRE: Evaluation of Normalized Taylor Coefficients of an Analytic Function*, Comm. ACM **14** (1971), 669–675.

[31] P.A. Markowich, P. Pietra and C. Pohl, *Weak limits of finite difference schemes for Schrödinger–type equations*, submitted to Numer. Math., 1997.

[32] T.A. Manteuffel and A.B. White Jr., *The numerical solution of second order boundary value problems on nonuniform meshes*, Math. Comput. **47** (1986), 511–535.

[33] B. Mayfield, *Non–local boundary conditions for the Schrödinger equation*, Ph.D. thesis, University of Rhode Island, Providence, RI, 1989.

[34] S.T. McDaniel and D. Lee, *A finite–difference treatment of interface conditions for the parabolic wave equation: The horizontal interface*, J. Acoust. Soc. Am. **71** (1982), 855–858.

[35] J.S. Papadakis, *Impedance formulation of the bottom boundary condition for the parabolic equation model in underwater acoustics*, NORDA Parabolic Equation Workshop, NORDA Tech. Note 143, 1982.

[36] J.S. Papadakis, M.I. Taroudakis, P.J. Papadakis and B. Mayfield, *A new method for a realistic treatment of the sea bottom in the parabolic approximation*, J. Acoust. Soc. Am. **92** (1992), 2030–2038.

[37] J.S. Papadakis, *Impedance Bottom Boundary Conditions for the Parabolic–Type Approximations in Underwater Acoustics*, in Advances in Computer Methods for Partial Differential Equations VII, eds. R. Vichnevetsky, D. Knight, and G. Richter, IMACS, New Brunswick, NJ, 1992, pp. 585–590.

[38] M. Reed and B. Simon, *Methods of Modern Mathematical Physics, Part I: Functional Analysis*, Academic Press, New York, 3rd ed. 1987.

[39] F. Schmidt and P. Deuflhard, *Discrete transparent boundary conditions for the numerical solution of Fresnel's equation*, Comput. Math. Appl. **29** (1995), 53–76.

[40] F. Schmidt and D. Yevick, *Discrete transparent boundary conditions for Schrödinger–type equations*, J. Comp. Phys. **134** (1997) 96–107.

[41] F. Schmidt, *Construction of discrete transparent boundary conditions for Schrödinger–type equations*, Preprint SC 97–60, ZIB Berlin (1997).

[42] G. Szegö, *Orthogonal Polynomials*, Amer. Math. Soc. Colloquium Publications 23, 3rd ed. 1967.

[43] F.D. Tappert, *The parabolic approximation method*, in *Wave Propagation and Underwater Acoustics*, Lecture Notes in Physics 70, eds. J.B. Keller and J.S. Papadakis, Springer, New York, 1977, pp. 224–287.

[44] D.J. Thomson, *Wide–angle parabolic equation solutions to two range–dependent benchmark problems*, J. Acoust. Soc. Am. **87** (1990), 1514–1520.

[45] D.J. Thomson and M.E. Mayfield, *An exact Radiation Condition for Use with the A Posteriori PE Method*, J. Comp. Acous. **2** (1994), 113–132.

[46] R. Vichnevetsky, *Wave propagation and reflection in irregular grids for hyperbolic equations*, Appl. Numer. Math. **3** (1987), 133–166.

[47] B.T. Wetton and G.H. Brooke, *One–way wave equations for seismoacoustic propagation in elastic waveguides*, J. Acoust. Soc. Am. **87** (1990), 624–632.